Characterization of individual molecular adsorption geometries by atomic force microscopy: Cu-TCPP on rutile TiO_2 (110)

Res Jöhr, Antoine Hinaut, Rémy Pawlak, Ali Sadeghi' , Santanu Saha, Stefan Goedecker, Bartosz Such, Marek Szymonski, Ernst Meyer' , and Thilo Glatzel

Citation: The Journal of Chemical Physics **143**, 094202 (2015); doi: 10.1063/1.4929608
View online: http://dx.doi.org/10.1063/1.4929608
View Table of Contents: http://aip.scitation.org/toc/jcp/143/9
Published by the American Institute of Physics

Characterization of individual molecular adsorption geometries by atomic force microscopy: Cu-TCPP on rutile TiO_2 (110)

Res Jöhr,[1] Antoine Hinaut,[1] Rémy Pawlak,[1] Ali Sadeghi,[2,a)] Santanu Saha,[1]
Stefan Goedecker,[1] Bartosz Such,[3] Marek Szymonski,[3] Ernst Meyer,[1,b)] and Thilo Glatzel[1]
[1]*Department of Physics, University of Basel, Klingelbergstrasse 82, 4056 Basel, Switzerland*
[2]*Physics Department, Shahid Beheshti University, G. C., Evin, 19839 Tehran, Iran*
[3]*Department of Physics, Jagiellonian University, Lojasiewicza 11, 30-348 Krakow, Poland*

(Received 30 June 2015; accepted 5 August 2015; published online 1 September 2015)

Functionalized materials consisting of inorganic substrates with organic adsorbates play an increasing role in emerging technologies like molecular electronics or hybrid photovoltaics. For such applications, the adsorption geometry of the molecules under operating conditions, e.g., ambient temperature, is crucial because it influences the electronic properties of the interface, which in turn determine the device performance. So far detailed experimental characterization of adsorbates at room temperature has mainly been done using a combination of complementary methods like photoelectron spectroscopy together with scanning tunneling microscopy. However, this approach is limited to ensembles of adsorbates. In this paper, we show that the characterization of individual molecules at room temperature, comprising the determination of the adsorption configuration and the electrostatic interaction with the surface, can be achieved experimentally by atomic force microscopy (AFM) and Kelvin probe force microscopy (KPFM). We demonstrate this by identifying two different adsorption configurations of isolated copper(II) meso-tetra (4-carboxyphenyl) porphyrin (Cu-TCPP) on rutile TiO_2 (110) in ultra-high vacuum. The local contact potential difference measured by KPFM indicates an interfacial dipole due to electron transfer from the Cu-TCPP to the TiO_2. The experimental results are verified by state-of-the-art first principles calculations. We note that the improvement of the AFM resolution, achieved in this work, is crucial for such accurate calculations. Therefore, high resolution AFM at room temperature is promising for significantly promoting the understanding of molecular adsorption. [http://dx.doi.org/10.1063/1.4929608]

I. INTRODUCTION

The concept of functionalized surfaces, where the substrate characteristics are modified by molecules with dedicated properties, offers a vast amount of potential applications like hybrid photovoltaics, molecular sensors, photocatalysts, or molecular electronics.[1–4] Even though this approach is not limited with respect to the choice of substrates, the wide band gap semiconductor TiO_2 has become one of the most relevant and studied substrates in the field.[5] Its absorption of light can be expanded with the help of a dye molecule. In this case, the photon is absorbed by the dye and the excited electron is injected to the conduction band of the TiO_2. This spectral sensitization plays an important role in dye-sensitized solar cells (DSCs).[2]

The performance or even the working mechanism of devices based on functionalized materials depends on the structure of the molecule attached to the substrate. Besides the desired effect that the substrate properties are modified, one has to consider that interaction with the substrate likely alters the properties of the molecule as well. For example, the key interfacial charge transfer processes in DSCs, like electron injection and recombination, depend on the adsorption mode of the sensitizer. For metalloporphyrins, it has been found that the distance of the metal core from the TiO_2 substrate and the tilt angle of the molecule with respect to the surface are crucial.[6,7] The electron injection might also be influenced by the resulting dipole moment normal to the surface.[8] Density functional theory (DFT) calculations have further shown that the interfacial dipole can change the position of the TiO_2 conduction band, which has direct influence on the open circuit voltage of DSCs.[9,10]

In a real device, several anchoring geometries are possible, due to the fact that they are often based on mesoporous substrates with different crystallographic surfaces and defects. Even on single crystal surfaces, different adsorption geometries are possible depending, e.g., on the substrate topography as well as the size and flexibility of the molecule. In addition, the adsorption modes are likely to depend also on experimental conditions, such as temperature. In order to get new insights into the fundamental physics at the interface, it is thus necessary to study single molecules under conditions similar to the ones under device operation. Recognizing the need for a better understanding of these interfaces, the adsorption modes of mainly small molecules on TiO_2 have been determined using synchrotron based techniques like photoelectron spectroscopy, surface X-ray diffraction, or X-ray photoelectron diffraction measurements.[11,12] Somehow, this methods are less suitable for systems with different adsorption modes, because

a)Formerly at Department of Physics, University of Basel, Klingelbergstrasse 82, 4056 Basel, Switzerland.
b)Electronic mail: ernst.meyer@unibas.ch

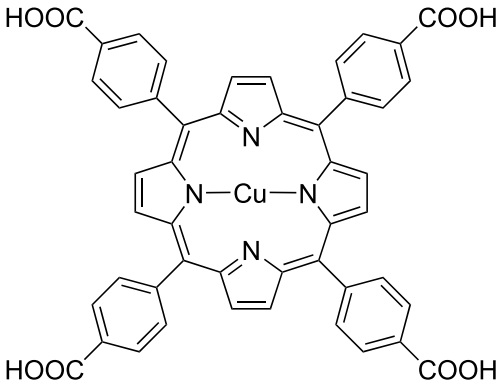

FIG. 1. Molecular structure of copper(II) meso-tetra (4-carboxyphenyl) porphyrin.

they measure the averaged properties of an ensemble. Thus, individual adsorbates at room temperature have only been measured by scanning probe methods.[13–17] For a more detailed understanding of the experimental results, they have often been combined with DFT calculations. However, the quality of the initial configurations deduced from the experiments determine the relevance of the DFT results. If the resolution of atomic force microscopy (AFM) and Kelvin probe force microscopy (KPFM) at room temperature could be increased, the DFT calculations would be improved with respect to speed and comparability with the experiment. Theoretically, this can be achieved using smaller oscillation amplitudes and stiffer cantilevers.[18] Both are feasible by using commercial cantilevers at the second flexural resonance.[19]

In this paper, we show that non-contact (nc) AFM at room temperature and under ultra-high vacuum (UHV) operating at the 2nd resonance is able to resolve the adsorption mode of isolated molecules as well as the substrate structure below. We demonstrate this by imaging isolated copper(II) meso-tetra (4-carboxyphenyl) porphyrin, so-called Cu-TCPP (Figure 1), adsorbed on the TiO_2 rutile (110) surface. High resolution topography images reveal two flat adsorption geometries, which have different adsorption sites and orientations with respect to the substrate surface. The interaction of the molecules with the surface is further assessed using KPFM. For verification, we compare the experimental results with DFT calculations and find that they are in good agreement.

II. METHODS

A. NC-AFM

Experiments were made with a home build UHV room temperature nc-AFM with a base pressure lower than $2 \cdot 10^{-11}$ mbars.[20] Measurements were done using silicon cantilevers (PPP-NCL, PPP-NCH, SSS-NCL from Nanosensors, Switzerland). Prior to measurement, cantilevers were prepared by thermal annealing (373 K, 1 h) and Ar^+ sputtering (680 eV, 90 s). Topography images were recorded using the resonance frequency shift as feedback signal.[21] During the measurement, the averaged contact potential difference (CPD) between tip and sample was compensated by applying a constant bias voltage to the sample. High resolution nc-AFM images were acquired on the second flexural mode ($f_2 \approx 950$ kHz) at an amplitude of $A_2 = 400$ pm. The second resonance was used because its high effective stiffness $k_2 \approx 1850\,\mathrm{N\,m^{-1}}$ was needed to reach stable measurement conditions at small amplitudes.[19]

B. KPFM

Experiments were done in the frequency modulation (FM) mode[22] using modulation frequencies of 200 Hz at an excitation amplitude of 700 mV. The bias for the CPD compensation was applied to the sample. Therefore, the image contrast of the applied bias has the same contrast as the work function.[23] Measurements were performed using PPP-NCL Pt cantilevers (Nanosensors, Switzerland) with a resonance frequency of $f_1 \approx 150$ kHz at an amplitude of $A_1 = 3$ nm. The cantilevers were prepared the same way as the ones used for nc-AFM measurements.

C. Sample preparation

A rutile TiO_2 (110) single crystal (MaTeck GmbH, Germany) was prepared by repeated cycles of Ar^+ sputtering (700 eV, 10 min) and subsequent annealing (1070 K, 15 min). The sample temperature was monitored using an infrared pyrometer (Impac IGA 140, LumaSense Technologies) measuring the temperature of the resistively heated silicon upon which the sample was mounted. Normally, the sample was cooled down within 5 min with the exception of the last cool down before the measurement. This lasted 30 min and was necessary in order to get well defined step edges. 5,10,15,20-tetrakis-(4-carboxyphenyl)-porphyrin-Cu(II) (Rare Chemicals GmbH, Germany) was evaporated during 2 min using a molecular evaporator (TCE-BSC, Kentax GmbH, Germany) operated at 600 K. The estimated sample temperature during deposition was around 400 K.

D. DFT calculations

The calculations were carried out within the generalized gradient approximation of DFT using homemade norm-conserving pseudopotentials.[24,25] We employed the BigDFT code[26] which enables us to apply periodic boundary conditions only along the two lateral directions but not along the third one, i.e., normal to the substrate surface.[27] Our model slab consisted of four trilayers each being a 4×9 cell. For such a large cell, we did the calculations only at the Γ point. The two layers at the bottom were kept frozen at their ideal crystal positions during geometry relaxations. Spin polarization was only included during test calculations using a model slab with two trilayers. The adsorption geometries were hardly influenced by the spin polarization and the binding energies were in the same range. Dispersion effects were included via the empirical pair potential of Grimme.[28] Molecular charge calculations were made using Bader charge analysis.[29,30]

III. RESULTS AND DISCUSSION

A. Surface of rutile TiO_2 (110)

The nc-AFM measurements revealed flat terraces with an average width of about 50 nm (Figure 2(a)). Step edges were along the $\langle 001 \rangle$ and $\langle 1\bar{1}1 \rangle$ directions. The fine structure on the

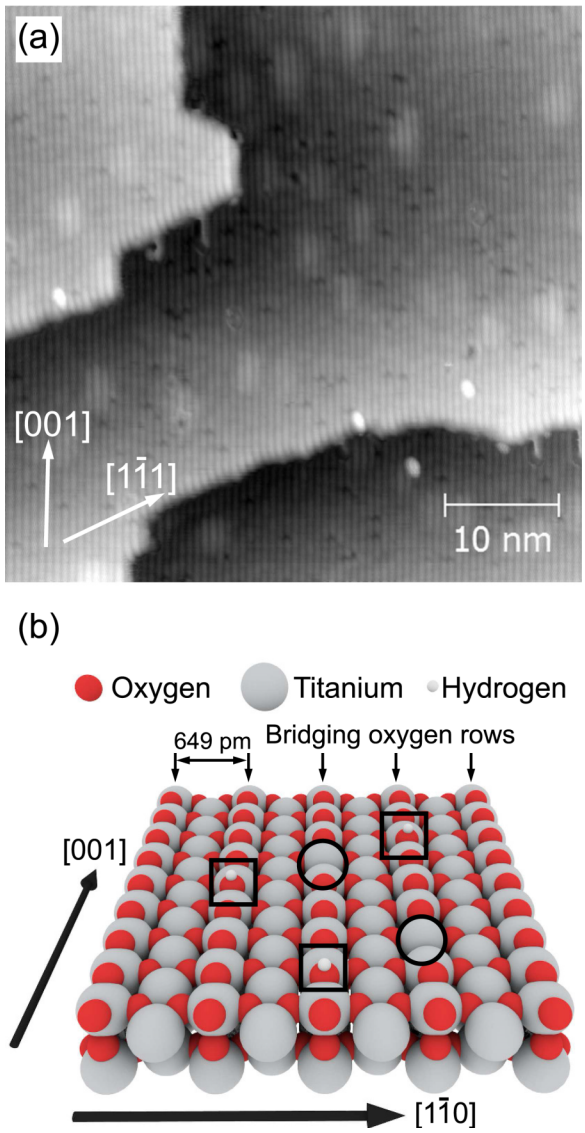

FIG. 2. Structure of the (1 × 1) reconstructed rutile TiO_2 (110) substrate: (a) nc-AFM topography showing oxygen rows along the [001] direction and step edges along the ⟨001⟩ and ⟨1$\bar{1}$1⟩ directions (f_2 = 1.974 MHz, A_2 = 400 pm, Δf = −71 Hz, Q = 8800). (b) Model of the rutile TiO_2 (110) surface with defects. Oxygen vacancies and hydrogen adatoms are marked with circles and squares, respectively.

terraces exhibited a stripe pattern along the [001] direction that is attributed to bridging oxygen rows.[5] The spacing between single bridging oxygen rows was about 650 pm. These experimental results are in good accordance with reported data on rutile TiO_2 (110) with a (1 × 1) reconstruction.[5] The sample was highly reduced due to the repeated sputtering/annealing cycles during sample preparation. Hence, defects such as oxygen vacancies and hydrogen adatoms were present (Figure 2). A model of the surface with defects is shown in Figure 2(b). The types of the defects were determined from nc-AFM images made with negative or neutral tip polarization.[31,32] In some regions, we could not detect defects at all, which is due to the influence of charged subsurface defects.[33] The ratio of the two aforementioned defects changed with time. At room temperature, residual water and hydrogen adsorbed continuously causing the accumulation of hydrogen adatoms on the surface.[34–36]

High resolution images showed different image contrasts, which is due to the fact that atomic resolution topography images depend strongly on the tip apex. For TiO_2, several imaging contrasts have been observed and explained by the apex termination and tip polarity.[31,32,37] It is important to note that the topography does no longer represent the correct relative heights of the individual surface atoms if the tip is polarized. Oxygen rows might even appear lower than the titanium rows then. Thus, the atomic species cannot be determined by their expected height. Nevertheless, the assignment of the atomic species on the TiO_2 surface is possible by considering that the known defects occur on the bridging oxygen rows.[38] Hence, identification of the adsorption sites of molecules is feasible no matter which contrast is obtained.

B. Adsorption geometries of Cu-TCPP

Evaporation of Cu-TCPP onto the hot substrate (400 K) led to deposition of isolated molecules (Figure 3(a)). The majority of the molecules were adsorbed on terraces, implying that the diffusion was suppressed due to strong interaction with the substrate. The molecules appeared as bright protrusions with a diameter of about 2 nm and a height of around 3 Å, indicating that the molecules lay flat on the surface. High resolution nc-AFM measurements revealed submolecular contrast that included contrast on the substrate as well (Figures 3(b) and 3(c)). The molecules aligned themselves with respect to the rows, resulting in two main orientations. One part of them had their Cu-cores on a bridging oxygen row and their carboxyphenyl substituents were in a 45° angle with respect to this row. Depending on the obtained contrast, they were sometimes only visible as squares. Therefore, we refer to this geometry as the square configuration (Figure 3(b)). The other molecules were rotated in plane by 45° with respect to the squares, having their axes along and perpendicular to the oxygen rows with their central copper atom positioned on a titanium row. They appeared as crosses. Hence, we denote this binding mode as the cross configuration (Figure 3(c)). Apparent height profiles for the two configurations are shown in Figure 3(d). The corresponding heights were calculated from the profiles of 13 molecules per configuration. The averaged heights were h_+ = 3.02 ± 0.13 Å and $h_□$ = 2.50 ± 0.21 Å for the cross and square orientation, respectively. Therefore, it was possible to distinguish the two adsorption configurations even on large scale images. Most of the molecules were found in these two symmetric geometries depicted in Figures 3(e) and 3(f), respectively. Asymmetric binding modes like the tilted cross shown in Figure 3(b) were observed scarcely.

C. Stability of geometries

Some of the topography images revealed several noise lines or marks (Figure 4(a)). The number of these marks increased with decreasing tip sample distance. Therefore, these artifacts can be attributed to tip induced displacements of porphyrins.[39,40] In fact, the comparison of two consecutive images showed that molecules in the square configuration moved along the oxygen rows (Figure 4(b)). Only in rare cases, molecules were displaced across the rows even though this was

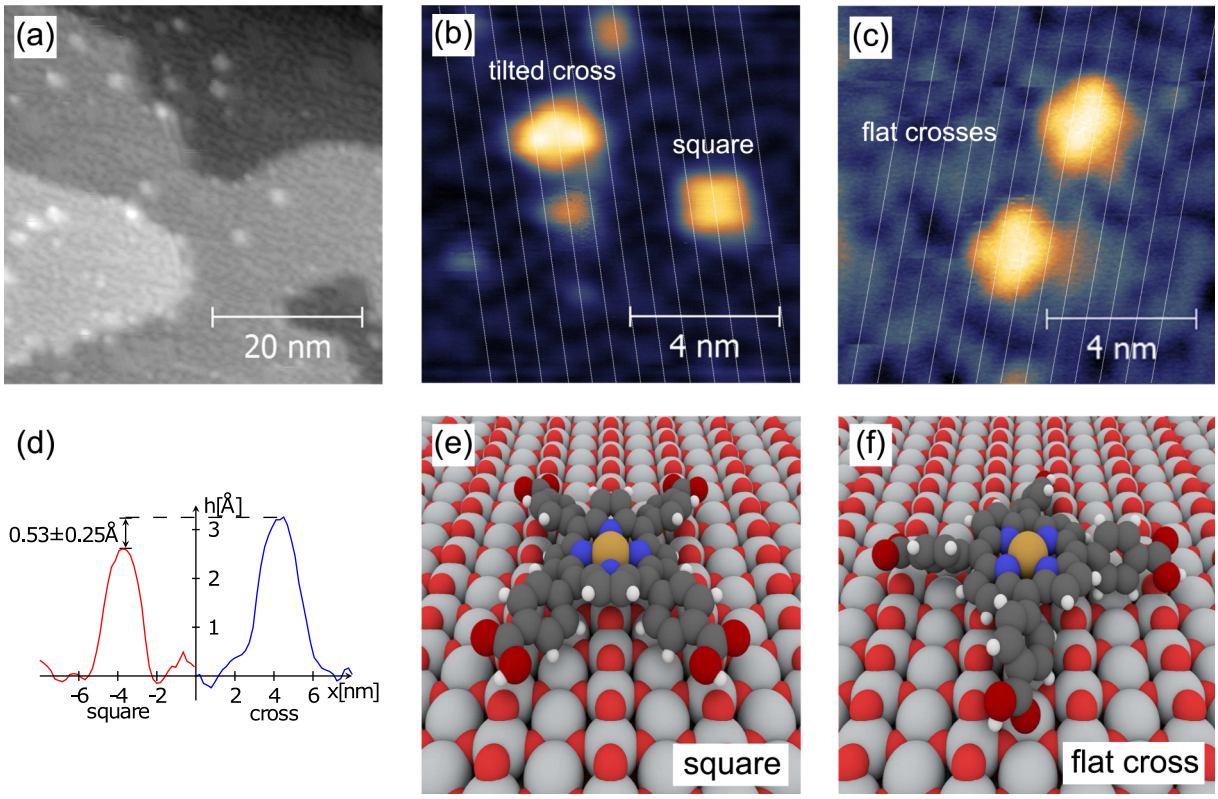

FIG. 3. Different binding geometries of Cu-TCPP on rutile TiO_2 (110): (a) large scale nc-AFM topography image ($f_2 = 1.001$ MHz, $A_2 = 400$ pm, $\Delta f = -10$ Hz, $Q = 7529$). (b) and (c) High resolution images of different adsorption geometries ((b) $f_2 = 957.9$ kHz, $A_2 = 400$ pm, $\Delta f = -13$ Hz, $Q = 10\,441$, (c) $f_2 = 1.001$ MHz, $A_2 = 400$ pm, $\Delta f = -10$ Hz, $Q = 7529$). Bridging oxygen rows are indicated with white lines. (d) Typical height profiles for the flat square and cross adsorption mode. (e) and (f) Proposed models for the symmetric square and cross orientations.

the fast scan direction. Hence, the preferential displacement was along the bridging oxygen rows. Movement of the cross configuration was not observed. They remained stable until the tip was too close so that the molecules were picked up.

D. KPFM measurements

The local contact potential difference (LCPD) between the sample and the tip was measured using frequency modulation Kelvin probe force microscopy (FM-KPFM), while the bias was applied to the sample.[22] Figures 5(a) and 5(b) show the topography and the corresponding slope corrected LCPD map, respectively. The correction of the background slope was justified by the presence of polarized step edges.[41] In the LCPD map, single Cu-TCPP molecules were clearly visible as dark features, indicating that the local work function on them was lowered by about 25 mV. There was no major difference between the two configurations. The lower local work function on the Cu-TCPP can be attributed to an interface dipole caused by electron transfer from the Cu-TCPP to the substrate.[42,43]

E. DFT calculations

The adsorption geometries inspired by AFM were used as input for DFT calculations in order to determine the exact adsorption site as well as the protonation state of the carboxylic acid anchors. For the latter, we took into account that a carboxylic proton is either retained on the dye or transferred to a bridging oxygen nearby.[44] We focused our calculations on the two symmetric configurations. For most of the calculations, we considered the surface to be free of defects. For the square configuration, we accounted for the case of an oxygen vacancy below the central copper atom. We legitimate this assumption as follows. We already noted that hydrogen adatoms were accumulating with time, meaning that the amount of hydrogen adatoms was supposed to be much lower during the evaporation than indicated by our images. Hence, during the evaporation, the majority of the defects were oxygen vacancies. However, both defects, oxygen vacancies that might react with the carboxylic acid and hydrogen adatoms, are supposed to lead to asymmetric adsorption geometries. Thus, for the study of symmetric geometries, it should be sufficient to consider the perfect rutile TiO_2 (110) surface for most of the cases.

The expected structures were relaxed by DFT calculations using the generalized gradient approximation. Van der Waals forces were included using empirical pair potentials. The calculated heights of the molecules with respect to the plane through the unrelaxed bridging oxygen rows are given in Table I. The copper atom, which reflects the center of the molecule, is about 0.7 Å higher in the cross geometries than in the squares. The average heights, calculated as the mean value of all the atoms of the porphyrin, differ by approximately 0.4 Å. In a first approximation, these height differences can be interpreted physically as consequence of the electrostatic interaction between the positively charged copper core of the porphyrin and the surface atom below, which is either a negative bridging oxygen or a positive titanium atom. The height

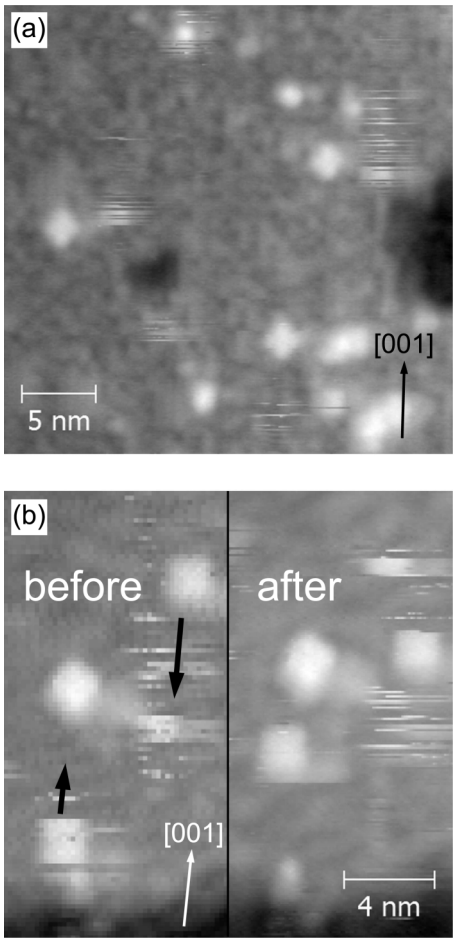

FIG. 4. (a) AFM image with noise lines ($f_2 = 1.001$ MHz, $A_2 = 400$ pm, $\Delta f = -10$ Hz, $Q = 7991$). (b) Two consecutive nc-AFM pictures showing the displacement of molecules in the square configuration ($f_2 = 1.001$ MHz, $A_2 = 400$ pm, $\Delta f = -9$ Hz, $Q = 7166$). The black arrows indicate the direction of the tip induced molecule movement.

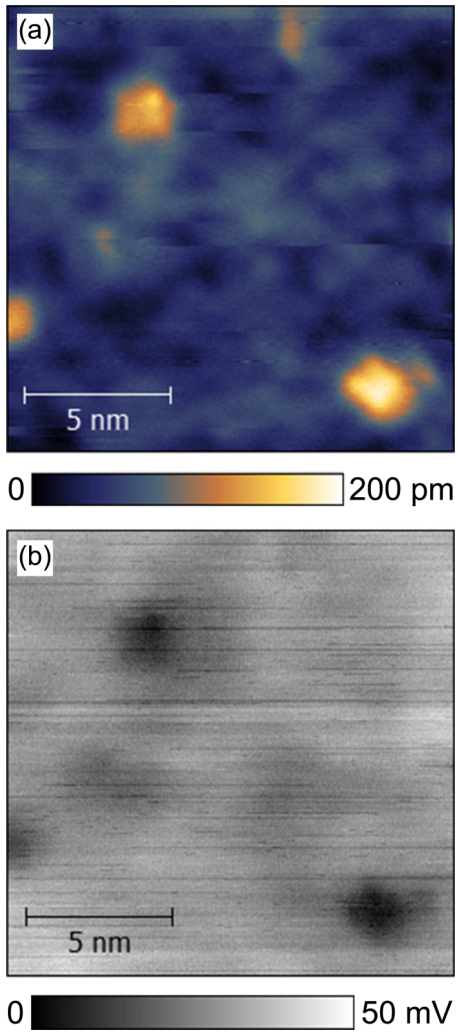

FIG. 5. Topography image (a) and slope corrected LCPD map (b) of two differently bound Cu-TCPP molecules measured simultaneously using FM-KPFM with a platinum coated cantilever ($f_1 = 149.3$ kHz, $\Delta f = -115$ Hz, $A_1 = 3$ nm, $Q = 20\,396$, $V_{mod} = 700$ mV, $f_{mod} = 200$ Hz).

difference between the two orientations is comparable to the one from AFM ($h_+ = 3.02 \pm 0.13$ Å and $h_\square = 2.50 \pm 0.21$ Å). We assume that the experimentally determined height difference was mainly caused by the real topography. This is further corroborated by the observation that the charging state of the two orientations was similar, as indicated by KPFM and DFT.

In order to determine the configuration that fits best with our experimental results, we calculated the binding energies between the molecule and the substrate as

$$E_B = E_{mol@sub} - (E_{mol} + E_{sub}), \quad (1)$$

where E_{mol} and E_{sub} are the calculated energies for the isolated molecule and substrate slab, respectively. $E_{mol@sub}$ is the energy of the combined molecule-titania system after adsorption. The three geometries shown in Figure 6 have binding energies around −3.5 eV. They are supposed to be stable at room temperature. The other configurations have lower binding energies that are not likely to yield stable adsorption modes. The strongest binding is found for the fully protonated configurations. The preferred square configuration is on the defect-free surface

TABLE I. Properties of different Cu-TCPP adsorption geometries calculated using DFT.

	Height (Å)					
Configuration	Cu	Average	E_B[a] (eV)		ΔQ_{mol} (e)	p_z (D)
Square	2.51	2.55	−3.56	(−3.88)	−0.85	16.9
Square on vacancy	2.61	2.57	−2.25		−0.59	14.7
Cross	3.22	2.93	−3.65	(−3.04)	−0.70	26.3
Cross partly deprot.	3.25	2.95	−3.36		−1.55	22.1
Cross fully deprot.	3.24	2.99	+0.01		−2.85	16.2

[a]Values in brackets denote the van der Waals contribution.

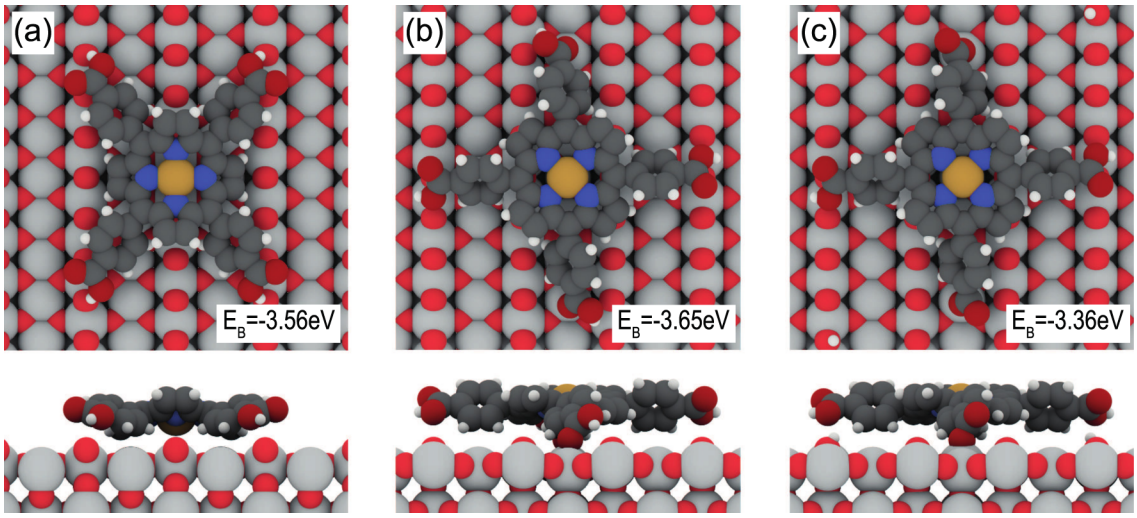

FIG. 6. Top and side views of the relaxed structures from the DFT calculations that fit best with the nc-AFM images: (a) square configuration without defect, (b) fully protonated cross configuration, and (c) partly deprotonated cross. For the latter, the released protons were put on bridging oxygen atoms (see top right and bottom left corners of the figure).

and is centered on a bridging oxygen row (Figure 6(a)). This geometry shows an attractive electrostatic interaction of the copper core and the polarized carboxylic protons with the bridging oxygen atoms. However, the overall charge distribution of the Cu-TCPP results in a net repulsive electrostatic force contribution. The entire attractive interaction is caused by van der Waals forces, whose amount is larger than the total binding energy E_B and is thus able to compensate for the repulsive part. The cross configurations are centered on a fivefold coordinated titanium atom (Figures 6(b) and 6(c)). Their carboxylic acid anchors that are on the center titanium row can form covalent bonds to the surface titanium atoms below. The protonated cross shown in Figure 6(b) is the most stable configuration. Deprotonation of the covalently bound carboxylic groups does not enhance the binding strength (Figure 6(c)).

At the first glance, this is contrary to the common assumption that carboxylic acids tend to deprotonate on titania.[12] Somehow, these reports consider small molecules where the carboxylic acid is actually found to bind preferentially in a bidentate mode. This mode might not be possible for large molecules because of strong van der Waals interaction.[16,17] These forces promote flat adsorption geometries where the bidentate mode is sterically hindered. Furthermore, it was found by Bates *et al.* that deprotonation is less favored for monodentate binding modes because of lack of resonance stabilization.[44]

The calculated binding energies agree with the AFM results on the fact that both orientations should be present. The stability of the two orientations with respect to tip induced displacement can be explained by the nature of the molecule surface interaction. The crosses can have covalent bonds and are therefore statistically less mobile than the squares that are mainly bound by van der Waals forces.

The influence of the adsorption geometry on the electronic properties of the interface was assessed by calculating the interface dipole moment normal vector to the surface p_z and the charge transfer from the molecule to the surface ΔQ_{mol} (Table I). The latter is given by the difference of the molecular charge of the free molecule, which includes charging due to possible deprotonation, and the adsorbed molecule. For all the considered geometries, charge is transferred to the substrate upon adsorption. The interface has thus a dipole moment, which points away from the surface. This is consistent with our KPFM measurements. The calculated dipoles indicate that the cross configurations should have an even lower LCPD than the square configurations. Somehow, we cannot see this difference in the KPFM images. The measurements were performed with a platinum coated silicon tip with a rather large tip apex. The radius of tip curvature was larger than 15 nm. The oscillation amplitude was 3 nm. Therefore, our experimental values were subject to considerable averaging by the tip shape but also by the oscillation amplitude.[45–47] This limited the sensibility for short range electrostatic forces and thus prevented to resolve the expected LCPD difference between the two configurations. Nevertheless, FM-KPFM gives qualitative information about the surface dipole. Furthermore, the authors expect that the resolution of FM-KPFM is improvable by the choice of the tip as well as the oscillation amplitude. The second flexural resonance might be applied in future as well.

IV. CONCLUSION

We demonstrated the determination of Cu-TCPP binding geometries and adsorption sites on rutile TiO_2 (110) at room temperature using nc-AFM at the second flexural resonance of the cantilever. AFM images revealed two configurations that were differently oriented with respect to the bridging oxygen rows. Further characterization of individual configurations was achieved by KPFM and indicated that there is a charge transfer to the surface upon adsorption leading to an interfacial dipole moment. The experimental results were verified and further investigated with DFT calculations. Three of the relaxed structures as well as their calculated properties, i.e., binding energy, height, and dipole moment are in good agreement with the experimental observations. Our experimental approach gives valuable information for the application of the investigated

system in DSCs. The dipole moment pointing away from the surface might slow down the electron injection to the conduction band of the TiO_2, thus limiting the device performance. This is in agreement with studies on similar systems like phthalocyanines, where it has been suggested that the strong interaction with the surface might bleach the photo-activity of the adsorbates.[17,48] We emphasize that these findings can be deduced from the experimental results alone. Thus, the study of individual molecular adsorption modes at room temperature is feasible by AFM and KPFM and promising that these methods will significantly contribute to a deeper understanding in future studies of functionalized surfaces.

ACKNOWLEDGMENTS

The authors thank Professor Edwin Constable and Professor Catherine Housecroft from the chemistry department of the University of Basel for fruitful discussions. The Swiss National Science Foundation (SNF), the Swiss Nanoscience Institute (SNI), and the Polish-Swiss Research Programme under Grant No. PSPB-085/2010 are acknowledged for financial support. We further acknowledge computer time at the Swiss National Supercomputing Centre (CSCS) under Project No. s499.

[1]M. S. Wrighton, Science **231**, 32 (1986).
[2]B. O'Regan and M. Grätzel, Nature **353**, 737 (1991).
[3]M. K. Nazeeruddin, D. Di Censo, R. Humphry-Baker, and M. Grätzel, Adv. Funct. Mater. **16**, 189 (2006).
[4]W. Liu, S. N. Filimonov, J. Carrasco, and A. Tkatchenko, Nat. Commun. **4**, 2569 (2013).
[5]U. Diebold, Surf. Sci. Rep. **48**, 53 (2003).
[6]H. Imahori, S. Kang, H. Hayashi, M. Haruta, H. Kurata, S. Isoda, S. E. Canton, Y. Infahsaeng, A. Kathiravan, T. Pascher, P. Chabera, A. P. Yartsev, and V. Sundström, J. Phys. Chem. A **115**, 3679 (2011).
[7]J. Rochford, D. Chu, A. Hagfeldt, and E. Galoppini, J. Am. Chem. Soc. **129**, 4655 (2007).
[8]A. Henning, G. Günzburger, R. Jöhr, Y. Rosenwaks, B. Bozic-Weber, C. E. Housecroft, E. C. Constable, E. Meyer, and T. Glatzel, Beilstein J. Nanotechnol. **4**, 418 (2013).
[9]F. De Angelis, S. Fantacci, A. Selloni, M. Grätzel, and M. K. Nazeeruddin, Nano Lett. **7**, 3189 (2007).
[10]E. Ronca, M. Pastore, L. Belpassi, F. Tarantelli, and F. De Angelis, Energy Environ. Sci. **6**, 183 (2013).
[11]C. L. Pang, R. Lindsay, and G. Thornton, Chem. Rev. **113**, 3887 (2013).
[12]C. L. Pang, R. Lindsay, and G. Thornton, Chem. Soc. Rev. **37**, 2328 (2008).
[13]K. Fukui, H. Onishi, and Y. Iwasawa, Chem. Phys. Lett. **280**, 296 (1997).
[14]A. Tekiel, J. S. Prauzner-Bechcicki, S. Godlewski, J. Budzioch, and M. Szymonski, J. Phys. Chem. C **112**, 12606 (2008).
[15]A. Sasahara, H. Uetsuka, T. Ishibashi, and H. Onishi, Appl. Surf. Sci. **188**, 265 (2002).
[16]A. Greuling, P. Rahe, M. Kaczmarski, A. Kühnle, and M. Rohlfing, J. Phys.: Condens. Matter **22**, 345008 (2010).
[17]S. Godlewski and M. Szymonski, Int. J. Mol. Sci. **14**, 2946 (2013).
[18]F. J. Giessibl, Rev. Mod. Phys. **75**, 949 (2003).
[19]S. Kawai, S. Kitamura, D. Kobayashi, S. Meguro, and H. Kawakatsu, Appl. Phys. Lett. **86**, 193107 (2005).
[20]L. Howald, E. Meyer, R. Lüthi, H. Haefke, R. Overney, H. Rudin, and H. Güntherodt, Appl. Phys. Lett. **63**, 117 (1993).
[21]T. R. Albrecht, P. Grütter, D. Horne, and D. Rugar, J. Appl. Phys. **69**, 668 (1991).
[22]S. Kitamura and M. Iwatsuki, Appl. Phys. Lett. **72**, 3154 (1998).
[23]S. Sadewasser, "Experimental technique and working modes," in *Kelvin Probe Force Microscopy*, edited by S. Sadewasser and T. Glatzel (Springer, 2012), pp. 7–24.
[24]C. Hartwigsen, S. Goedecker, and J. Hutter, Phys. Rev. B **58**, 3641 (1998).
[25]A. Willand, Y. O. Kvashnin, L. Genovese, A. Vazquez Mayagoitia, A. K. Deb, A. Sadeghi, T. Deutsch, and S. Goedecker, J. Chem. Phys. **138**, 104109 (2013).
[26]L. Genovese, A. Neelov, S. Goedecker, T. Deutsch, S. A. Ghasemi, A. Willand, D. Caliste, O. Zilberberg, M. Rayson, A. Bergman, and R. Schneider, J. Chem. Phys. **129**, 014109 (2008).
[27]L. Genovese, T. Deutsch, and S. Goedecker, J. Chem. Phys. **127**, 054704 (2007).
[28]S. Grimme, J. Comput. Chem. **27**, 1787 (2006).
[29]R. F. Bader, *Atoms in Molecules* (Wiley Online Library, 1990).
[30]G. Henkelman, A. Arnaldsson, and H. Jónsson, Comput. Mater. Sci. **36**, 354 (2006).
[31]J. V. Lauritsen, A. S. Foster, G. H. Olesen, M. C. Christensen, A. Kühnle, S. Helveg, J. R. Rostrup-Nielsen, B. S. Clausen, M. Reichling, and F. Besenbacher, Nanotechnology **17**, 3436 (2006).
[32]R. Bechstein, C. González, J. Schütte, P. Jelínek, R. Pérez, and A. Kühnle, Nanotechnology **20**, 505703 (2009).
[33]J. Onoda, C. L. Pang, A. Yurtsever, and Y. Sugimoto, J. Phys. Chem. C **118**, 13674 (2014).
[34]S. Wendt, J. Matthiesen, R. Schaub, E. K. Vestergaard, E. Lægsgaard, F. Besenbacher, and B. Hammer, Phys. Rev. Lett. **96**, 066107 (2006).
[35]Z. Zhang, O. Bondarchuk, B. D. Kay, J. M. White, and Z. Dohnálek, J. Phys. Chem. B **110**, 21840 (2006).
[36]C. L. Pang, A. Sasahara, H. Onishi, Q. Chen, and G. Thornton, Phys. Rev. B **74**, 073411 (2006).
[37]G. H. Enevoldsen, H. P. Pinto, A. S. Foster, M. C. R. Jensen, A. Kühnle, M. Reichling, W. A. Hofer, J. V. Lauritsen, and F. Besenbacher, Phys. Rev. B **78**, 045416 (2008).
[38]S. Wendt, R. Schaub, J. Matthiesen, E. Vestergaard, E. Wahlström, M. Rasmussen, P. Thostrup, L. Molina, E. Lægsgaard, I. Stensgaard, B. Hammer, and F. Besenbacher, Surf. Sci. **598**, 226 (2005).
[39]M. Watkins, T. Trevethan, A. L. Shluger, and L. N. Kantorovich, Phys. Rev. B **76**, 245421 (2007).
[40]B. Such, T. Trevethan, T. Glatzel, S. Kawai, L. Zimmerli, E. Meyer, A. L. Shluger, C. H. M. Amijs, P. de Mendoza, and A. M. Echavarren, ACS Nano **4**, 3429 (2010).
[41]A. Sasahara, H. Uetsuka, and H. Onishi, Surf. Sci. **529**, L245 (2003).
[42]A. Sasahara, C. L. Pang, and H. Onishi, J. Phys. Chem. B **110**, 17584 (2006).
[43]M. Ikeda, N. Koide, L. Han, A. Sasahara, and H. Onishi, J. Phys. Chem. C **112**, 6961 (2008).
[44]S. Bates, G. Kresse, and M. Gillan, Surf. Sci. **409**, 336 (1998).
[45]S. Sadewasser, C. Leendertz, F. Streicher, and M. C. Lux-Steiner, Nanotechnology **20**, 505503 (2009).
[46]R. Baier, C. Leendertz, M. C. Lux-Steiner, and S. Sadewasser, Phys. Rev. B **85**, 165436 (2012).
[47]A. Sadeghi, A. Baratoff, S. A. Ghasemi, S. Goedecker, T. Glatzel, S. Kawai, and E. Meyer, Phys. Rev. B **86**, 075407 (2012).
[48]F. Fuchs, M. Linares, C. de Vet, P. Leclère, R. Demadrille, and B. Grévin, Adv. Mater. **26**, 6416 (2014).